8. Moore, M. G. & Meystre, P. Theory of superradiant scattering of laser light from Bose-Einstein condensates. Preprint cond-mat/9905425 at ⟨http://xxx.lanl.gov⟩ (1999).
9. Mewes, M.-O. *et al.* Bose-Einstein condensation in a tightly confining dc magnetic trap. *Phys. Rev. Lett.* **77,** 416–419 (1996).
10. Kozuma, M. *et al.* Coherent splitting of Bose-Einstein condensed atoms with optically induced Bragg diffraction. *Phys. Rev. Lett.* **82,** 871–875 (1999).
11. Stenger, J. *et al.* Bragg spectroscopy of a Bose-Einstein condensate. *Phys. Rev. Lett.* **82,** 4569–4573 (1999).
12. Hagley, E. W. *et al.* Measurement of the coherence of a Bose-Einstein condensate. *Phys. Rev. Lett.* **83,** 3112–3115 (1999).
13. Miesner, H.-J. *et al.* Bosonic stimulation in the formation of a Bose-Einstein condensate. *Science* **279,** 1005–1007 (1998).
14. Deng, L. *et al.* Four-wave mixing with matter waves. *Nature* **398,** 218–220 (1999).
15. Berman, P. R. (ed.) *Atom Interferometry* (Academic, New York, 1997).
16. Schmiedmayer, J. *et al.* Index of refraction of various gases for sodium matter waves. *Phys. Rev. Lett.* **74,** 1043–1047 (1995).
17. Stedman, G. E. *et al.* Ring-laser tests of fundamental physics and geophysics. *Rep. Prog. Phys.* **60,** 615–688 (1997).
18. Gustavson, T. L., Bouyer, P. & Kasevich, M. A. Precision rotation measurements with an atom interferometer gyroscope. *Phys. Rev. Lett.* **78,** 2046–2049 (1997).

Acknowledgements

We thank D. M. Stamper-Kurn for discussions. This work was supported by the Office of Naval Research, NSF, Joint Services Electronics Program, ARO, NASA, and the David and Lucile Packard Foundation. A.P.C. was supported by NSF, A.G. by DAAD, and T.P. by the Alexander von Humboldt Foundation.

Correspondence and requests for materials should be addressed to S.I. (e-mail: sinouye@mit.edu).

Weaker Gulf Stream in the Florida Straits during the Last Glacial Maximum

Jean Lynch-Stieglitz*, William B. Curry† & Niall Slowey‡

** Department of Earth and Environmental Sciences, Lamont-Doherty Earth Observatory, Palisades, New York 10964, USA*
† Woods Hole Oceanographic Institution, Woods Hole, Massachusetts 02543, USA
‡ Department of Oceanography, Texas A & M University, College Station, Texas 77843, USA

As it passes through the Florida Straits, the Gulf Stream consists of two main components: the western boundary flow of the wind-driven subtropical gyre and the northward-flowing surface and intermediate waters which are part of the 'global conveyor belt', compensating for the deep water that is exported from the North Atlantic Ocean[1]. The mean flow through the Straits is largely in geostrophic balance and is thus reflected in the contrast in seawater density across the Straits[2]. Here we use oxygen-isotope ratios of benthic foraminifera which lived along the ocean margins on the boundaries of the Florida Current during the Last Glacial Maximum to determine the density structure in the water and thereby reconstruct transport through the Straits using the geostrophic method—a technique which has been used successfully for estimating present-day flow[3]. Our data suggest that during the Last Glacial Maximum, the density contrast across the Florida Straits was reduced, with the geostrophic flow, referenced to the bottom of the channel, at only about two-thirds of the modern value. If the wind-driven western boundary flow was not lower during the Last Glacial Maximum than today, these results indicate a significantly weaker conveyor-belt component of the Gulf Stream compared to present-day values. Whereas previous studies based on tracers suggested that deep waters of North Atlantic origin were not widespread during glacial times, indicating either a relatively weak or a shallow overturning cell, our results provide evidence that the overturning cell was indeed weaker during glacial times.

The Florida Current, which flows through the Florida Straits (Fig. 1), is the southernmost part of the Gulf Stream. The average northward transport of the Florida Current is fairly well constrained by modern measurement at 30–32 Sv, and shows a seasonal variation with a range of 4.6 Sv as well as considerable variability on shorter timescales[4]. Schmitz and McCartney[1] assign an uncertainty of only 5% to the mean annual transport value of 31 Sv. The transport at the Florida Current includes 13 Sv of flow from the South Atlantic which travels northward in the Gulf Stream to the North Atlantic and ultimately compensates for the export of North Atlantic Deep Water (NADW). The other 17 Sv compensate for southward-flowing upper waters from the eastern portion of the wind-driven North-Atlantic subtropical gyre[1]. The strong tilts in the surfaces of constant temperature and density within the Florida Straits reflect the geostrophic adjustment of the density surfaces in the presence of the large velocities (Fig. 2a and b). The contrast in temperature and density across the Florida Current is large, and is well represented in the $\delta^{18}O$ of benthic foraminifera living in this region.

We can use the $\delta^{18}O$ from the calcite tests of foraminifera to estimate density because both the $\delta^{18}O$ of calcite ($\delta^{18}O_{calcite}$) and density increase as a result of increasing salinity or decreasing temperature. The dependence of seawater density on salinity and temperature is well known and will be constant throughout the ocean and through geological time. The dependence of $\delta^{18}O$ of foraminifera on the temperature of calcification is also fairly well constrained. The fractionation between calcite precipitated inorganically and the water in which it forms increases by about 0.2‰ for every 1 °C decrease in temperature[5], and the isotopic composition of calcitic benthic foraminifera in the genera *Planulina* and *Cibicidoides* show the same fractionation as measured in the experiments with inorganic calcite[3]. The relationship between $\delta^{18}O_{calcite}$ and salinity is more complex. The $\delta^{18}O_{calcite}$ reflects the $\delta^{18}O$ of the water in which the foraminifera grew. The $\delta^{18}O$ of sea water ($\delta^{18}O_{water}$) primarily reflects patterns of evaporation and freshwater influx to the surface of the ocean. Because salinity also reflects these patterns, salinity and $\delta^{18}O_{water}$ are often well correlated in the ocean. Although the exact relationship varies in different areas of the surface ocean[6], the vast majority of surface and warm subsurface waters ($T > 5$ °C) in the ocean have salinity and $\delta^{18}O_{water}$ values which scatter around a linear trend[3]. For times in the geological past, our ability to reconstruct density from the $\delta^{18}O_{calcite}$

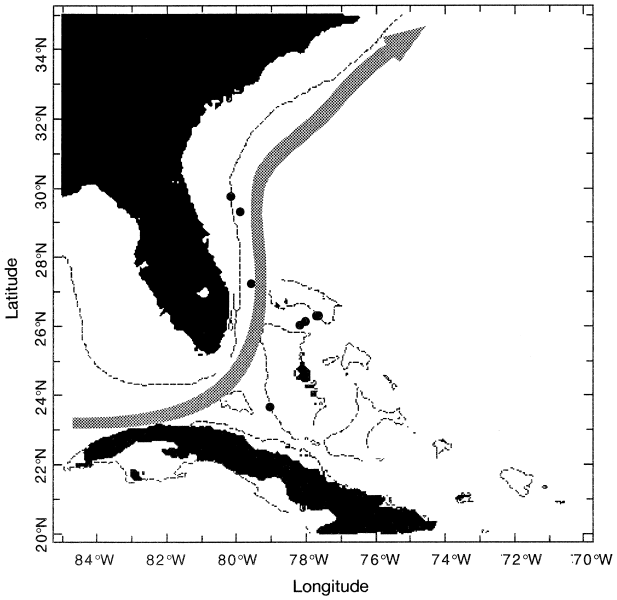

Figure 1 Location of sediment cores used in this study. The path of the Gulf Stream is indicated with the shaded arrow, and the depth of the 200-m isobath with a dashed line.

is most limited by our knowledge of the relationships between $\delta^{18}O_{water}$ and salinity, as well as the relationships between temperature and salinity. However, while the patterns of atmospheric and surface ocean circulation might have shifted in latitude, we still expect that there existed an evaporative subtropical gyre and a fresh sub-polar gyre even during the periods of maximum glaciation. By taking into consideration the presumed changes in ocean salinity and $\delta^{18}O_{water}$ due to sea-level change, and possible changes in the $\delta^{18}O$ of high-latitude precipitation, we can make an educated guess about the relationship between $\delta^{18}O_{water}$ and salinity for the glacial ocean. We can then determine the relationship between $\delta^{18}O_{calcite}$ and density for the glacial ocean (see Methods).

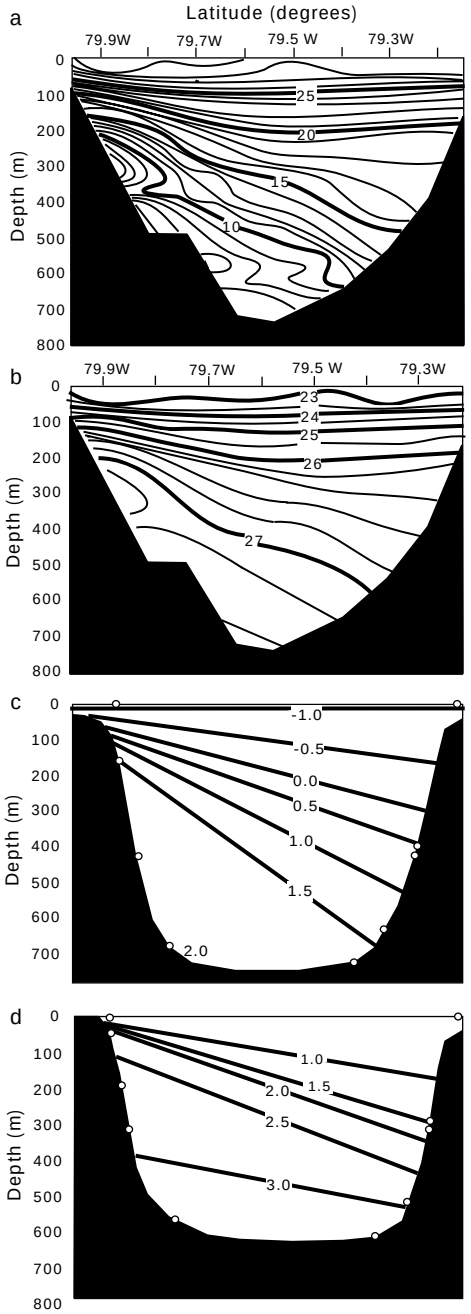

Figure 2 Observed and inferred hydrographic sections across the Florida Straits. **a**, **b**, Temperature in °C (**a**), density (σ_T) (**b**) observed across the Florida Straits at 27 N. Data are from the World Ocean Atlas CTD data set[29]. **c**, **d**, Section of $\delta^{18}O_{calcite}$ at a similar location for the Holocene (**c**) and LGM (**d**) oceans is inferred from the foraminiferal $\delta^{18}O_{calcite}$ shown in Figs 3 and 4. Black dots indicate the depths of the $\delta^{18}O_{calcite}$ measurements used in calculating the geostrophic flow. The LGM bathymetry has been adjusted upwards by 120 m to account for the sea level drop[26]. The Holocene $\delta^{18}O_{calcite}$ reconstruction (**c**) reflects the observed density structure. The LGM section (**d**) suggests the concentration of flow at shallower depths.

In order to reconstruct vertical profiles of $\delta^{18}O_{calcite}$, which can then be converted to density, we measured the $\delta^{18}O$ in individual benthic foraminifera (genera *Planulina* and *Cibicidoides*) from sediment cores on either side of the Florida Straits (Fig. 1). The benthic foraminifera data from four of the cores from the seaward (Bahamas) side of the current are from a previous study[7]. The isotopic data from the remaining cores used in this study are shown in Fig. 3. We used grouped $\delta^{18}O$ measurements from a planktonic foraminifera, *G. sacculifer*, to identify the Holocene and Last Glacial Maximum (LGM) levels in the cores and to constrain the surface ocean values of $\delta^{18}O_{calcite}$. The inferred distribution of $\delta^{18}O_{calcite}$ across the Florida Straits reconstructed from the core tops reflects the modern density structure in this region (Fig. 2). During the LGM there was very little contrast in $\delta^{18}O_{calcite}$ across the deeper portion of the Straits. If the LGM Florida Current was, like today's, largely baroclinic, this would imply very little northward flow at these depths. This is consistent with previous work which suggests little northward penetration of Antarctic Intermediate Water into the Caribbean during the LGM[8,9]. The tilting lines of constant $\delta^{18}O_{calcite}$ in the upper part of the section suggest that there was northward flow of surface waters through the glacial Florida Straits. To use the geostrophic method to calculate the flow from the vertical profiles of $\delta^{18}O_{calcite}$ (Fig. 4), we assume that the transport decreases to zero near the bottom of the channel, as is observed today. The core top profiles yield a transport of 30 Sv, in line with an estimate using a more extensive set of surface sediment data (32 Sv) (ref. 3) and modern estimates from physical oceanographic studies (30–32 Sv). Using our best estimate for the relationship between glacial $\delta^{18}O_{calcite}$ and density, the LGM profiles result in a transport estimate of 15–18 Sv. This reduced flow does not result simply from raising the reference level from 760 m (the depth of the channel today) to 640 m (the depth of the LGM channel). If we calculated the modern transport using a reference level of 640 m instead of 760 m, the flow is only reduced from 30 Sv to 27 Sv. By varying the assumptions that went into our estimate of the relationship between glacial $\delta^{18}O_{calcite}$ and density relationship within reasonable bounds, the LGM transport could have been as low as 14 Sv or as high as 21 Sv (see Methods). While today's flow is largely baroclinic we cannot rule out the possibility of a barotropic component to the flow during the last ice age. However, given that there is currently no evidence otherwise, we presume that, like today, the flow is small at the sill depth of the Florida Straits.

What could have lowered the transport through the Florida Straits during the LGM? While sedimentological evidence suggests increased aridity for the last glaciation, there is little direct evidence addressing wind strength in the glacial North Atlantic. However, atmospheric general circulation models driven by glacial boundary conditions suggest that the winds which drive the gyre circulation were either unchanged or slightly strengthened relative to today[10,11]. Stronger winds would have caused the wind-driven flow of upper waters through the Florida Straits to increase. A simple shift of the wind belts towards the Equator would also have caused an increase in the wind-driven transport. However, we cannot exclude the possibility of more complex changes in wind patterns which decrease the wind stress curl and, thus, the wind-driven Sverdrup transport at the latitude of the northernmost passage into the Caribbean. We believe that the simplest explanation for the reduction in the Florida Current is the reduction or absence of the interhemispheric component of the transport (13 of the 30 Sv flowing through the Florida Straits today), which compensates deep water formation in the North Atlantic.

There is substantial evidence that during the LGM, NADW did not dominate the deep Atlantic as it does today[12–14]. If there were no

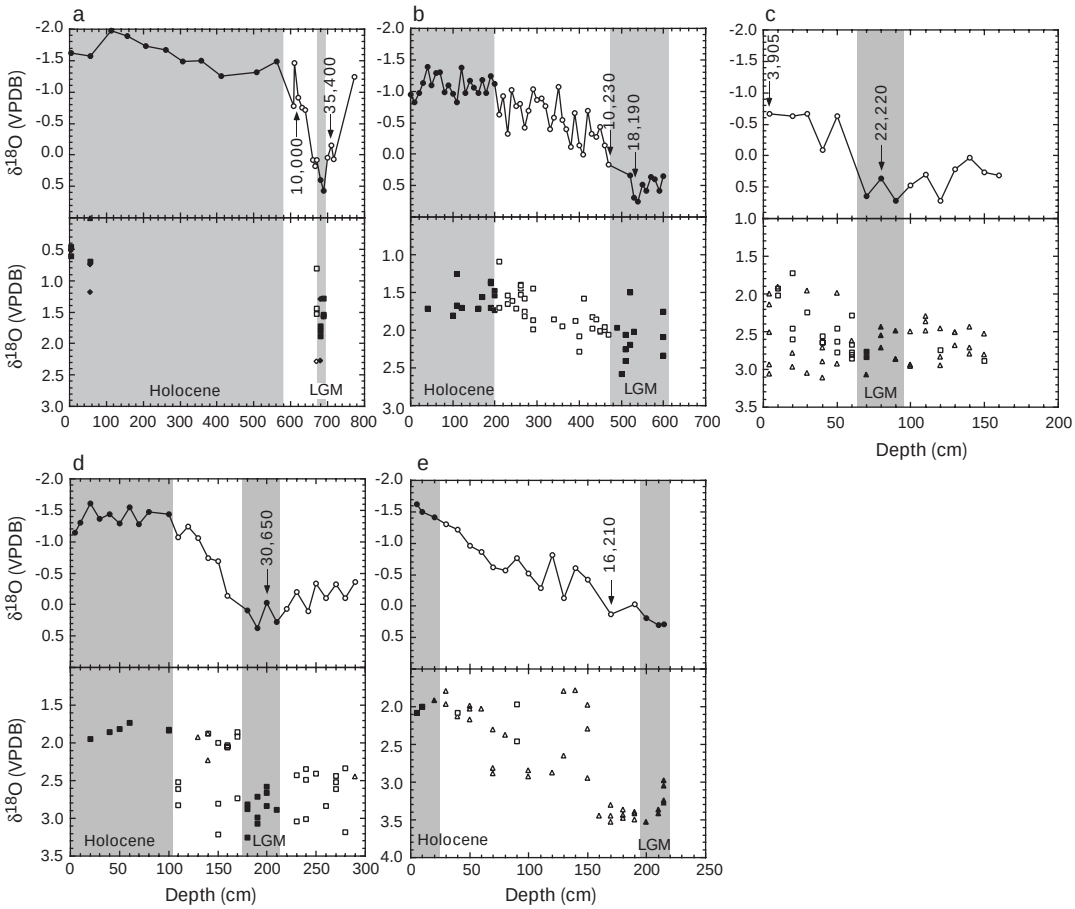

Figure 3 Isotopic measurements from sediment cores in this study. Oxygen-isotope ratios measured on the planktonic foraminifera *G. sacculifer* (circles) and individual benthic foraminifera, *P. ariminensis* (triangles), *C. pachyderma* (squares) and *C. foveolata* (diamonds). Filled symbols represent data contributing to LGM and Holocene averages. Radiocarbon dates (reservoir corrected) are also indicated at the corresponding depth in the cores. **a**, ODP Site 1008 at the Bahamas, 437 m. Planktonic foraminifera data and radiocarbon are from ref. 31. **b**, Florida slope core RC1-1, 174 m. **c**, Florida slope core RC1-2, 324 m. **d**, Florida slope core V7-13, 452 m. **e**, Florida slope core V3-149, 706 m. LGM, last glacial maximum.

deep-water formation in the North Atlantic, then the compensating northward surface-water transport would not have been present, explaining the observed decrease in transport through the Florida Straits. However, while NADW production appears to have decreased, the presence of a nutrient-depleted water mass at shallower depths (<2,000 m)[14,15] suggests a compensating increase in intermediate water export from the glacial Atlantic. Two- and three-dimensional ocean-circulation models do show a shift from deep to intermediate water production in the glacial North Atlantic under ice-age conditions (increased high-latitude freshwater flux)[16,17]. In these models, the production of Glacial North Atlantic Intermediate Water (GNAIW) is, like today's production of NADW, compensated by a northward flow of warm surface waters. The reduced western boundary transport we observe at the Florida Straits would require that the levels of nutrient depletion in the intermediate waters of the glacial Atlantic are achieved with a very weak overturning circulation. Sigman and Lehman[18] suggest that as little as 5 Sv of GNAIW formation are needed to explain the low Cd/Ca and high $\delta^{13}C$ observed in the glacial North Atlantic, as long as a significant fraction of this water is exported from the Atlantic. The export of GNAIW is supported by radiochemical[19] as well as nutrient-linked water mass tracers[20]. Other modelling studies[21] also suggest that a reduced meridional overturning circulation is consistent with LGM tracer distributions.

Alternatively, GNAIW may have been ventilated by a different mechanism altogether, one which did not involve the compensating northward flow of warm surface waters. Planktonic foraminifera assemblage data suggest a nearly zonal polar front separating the subtropics and subpolar gyres for the LGM North Atlantic[22]. This is consistent with the absence of a glacial 'North Atlantic Drift' bringing surface waters into high northern latitudes, and consequently, the presence of a well developed subpolar gyre. In addition, oxygen-isotope measurements in planktonic and benthic foraminifera suggest that surface waters in the region of the presumed LGM subpolar gyre are the only waters which could become dense enough to form the GNAIW[23]. If GNAIW were ventilated by deep convection in the subpolar gyre, the southward-flowing GNAIW would have been replaced primarily by northward-flowing intermediate waters which would have been too dense to have passed through the relatively shallow glacial Florida Straits.

The northward heat transport by the meridional overturning circulation is proportional to both the strength of the overturning circulation, and the temperature difference between the northward- and southward-flowing components. The very weak overturning circulation required if GNAIW was compensated by northward-flowing surface waters would result in a northward heat transport greatly reduced relative to today. Similarly, any scenario for the meridional circulation with cold intermediate waters compensating GNAIW export implies significantly less oceanic heat transport into the North Atlantic than today, and also less heat transport than predicted by the ocean models with a shallow but still strong conveyor circulation in the glacial Atlantic. □

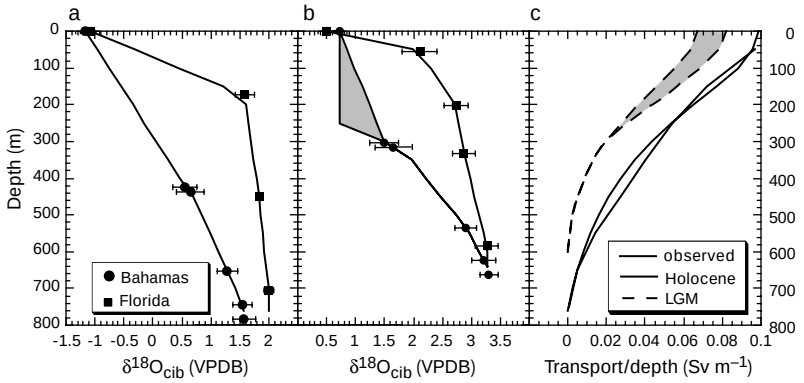

Figure 4 Modern and LGM oxygen isotope and transport profiles. **a**, **b**, Holocene (**a**) and LGM (**b**) $\delta^{18}O_{calcite}$ profiles. Error bars represent the 1σ standard deviation of the population of the $\delta^{18}O$ on individual foraminifera that went into the average for each core and level (Fig. 3). For the seaward (Bahamas) profile we show both a linear interpolation (minimum flow estimate) between the shallowest benthic foraminiferal data point and the surface, and an interpolation with a very deep mixed layer (maximum flow estimate). **c**, The vertical distribution of transports calculated using our best estimates of the relationship between density and $\delta^{18}O_{calcite}$. The total transport is 30 Sv for the Holocene (black line) and 16–19 Sv for the LGM (dashed lines). The vertical structure of today's transport through the Florida Straits at 27° N as determined by current profilers is also shown (grey line)[30].

Methods

Measurements on *G. sacculifer* for the cores shown in Fig. 3 were made at the Lamont-Doherty Earth Observatory on a Micromass Optima with Multiprep, except for ODP Site 1008 where measurements were made at Texas A&M University (ref. 31). *G. sacculifer* were picked from the 355–425-μm size fraction, and groups of 5–8 individuals were analysed. Measurements on individual benthic foraminifera (*P. ariminensis*, *C. pachyderma* and *C. foveolata*) were made at Woods Hole Oceanographic Institution using the methods described by Curry[24]. All oxygen-isotope measurements were converted to VPDB (Vienna PeeDee Belemnite) via NBS-19. Radiocarbon dates for the Florida Slope cores are from planktonic foraminifera and those for ODP Site 1008 are from bulk sediments; all radiocarbon dates are corrected for a 400-year reservoir effect.

Vertical profiles of $\delta^{18}O_{calcite}$ used to calculate geostrophic transport for the Holocene and the LGM are constructed as follows. The modern and LGM intervals for the sediment cores are identified based on the $\delta^{18}O$ stratigraphy of grouped analyses of the surface-dwelling planktonic foraminifera, *G. sacculifer*. Planktonic foraminiferal (*G. sacculifer*) $\delta^{18}O$ data from V7-13 (Fig. 3d) and 103GGC (Little Bahama Banks)[25] are used for the sea-surface data point in each profile. Average $\delta^{18}O_{calcite}$ for the Holocene and LGM sections of each core is computed from the measurements on the individual benthic foraminifera. Holocene and LGM averages from Slowey and Curry[7] are used for the deeper Bahamas cores. The core depths for the LGM data have been adjusted by 120 m to reflect the lowered sea level[26]. For the landward (Florida) profile, we linearly interpolate between the data at the core depths. For the seaward (Bahamas) profile, two different interpolations between the shallowest benthic foraminiferal data point and the surface are used, a linear interpolation (minimum flow estimate), and an interpolation with a very deep mixed layer (maximum flow estimate).

We then convert the Holocene $\delta^{18}O_{calcite}$ to density using the relationship for the modern ocean ($T > 5$ °C) described previously[3]. For the LGM, we assume that the relationship between temperature and salinity in the glacial ocean was similar to that of today, only that salinity was concentrated by a factor of 1.03 (about 1 psu) due to the build-up of continental ice. In addition, we assume that the mean ocean $\delta^{18}O$ increased by 1‰ for the same reasons[27]. We also assume that the relationship between $\delta^{18}O$ of sea water and salinity represents a mixing between sub-thermocline water and a fresh end member that has a salinity of zero and a $\delta^{18}O$ representative of precipitation in subpolar latitudes[6]. A study using an atmospheric general circulation model[28] suggests that during the LGM this subpolar precipitation was about 4‰ lower than today. We then propose that for warm waters in the glacial ocean $\delta^{18}O$ was related to salinity as follows: $\delta^{18}O = -19.3 + 0.52 \times \text{salinity}$. These changes result in a relationship between $\delta^{18}O_{calcite}$ and density, σ_t, for the glacial ocean of: $\sigma_t = 25.4 + 1.3\delta^{18}O_{calcite} - 0.12\delta^{18}O_{calcite}{}^2$. The geostrophic transport between the two profiles was calculated using the method described previously[3]. For the core tops, we assign a level of no motion at a depth of 760 metres, the depth of the strait at its most constricted point. For the LGM we adjust the level of no motion upward by 120 metres (to 640 metres) to account for the lowered sea surface. We obtain a transport of 30 Sv for the Holocene and 15–18 Sv for the LGM, using the relationship between density and $\delta^{18}O_{calcite}$ derived above, and the two different interpolated profiles for the seaward side of the Straits. We vary the assumed LGM mean ocean $\delta^{18}O$ change between 1 and 1.3‰ (ref. 26) higher than present, and the assumed LGM change in the $\delta^{18}O$ of high-latitude precipitation between 0‰ and 8‰ lower than present. A maximum transport of 21 Sv is obtained with a mean ocean $\delta^{18}O$ change of 1.3‰ and a $\delta^{18}O$ of high-latitude precipitation 8‰ lower than present. A minimum transport of 14 Sv is obtained with a mean ocean $\delta^{18}O$ change of 1‰ and a $\delta^{18}O$ of high-latitude precipitation the same as at present.

Received 4 May; accepted 12 October 1999.

1. Schmitz, W. J. & McCartney, M. S. On the North Atlantic Circulation. *Rev. Geophys.* **31,** 29–49 (1993).
2. Wust, G. Florida und Antillenstrom: Eine hydrodynamische Untersuchung. *Geographischnaturwiss, Reihe* **12,** 48 (1924).
3. Lynch-Stieglitz, J., Currey, W. & Slowey, N. A geostrophic transport estimate for the Florida Current from oxygen isotope composition of benthic foraminifera. *Paleoceanography* **14,** 360–373 (1999).
4. Larsen, J. C. Transport and heat-flux of the Florida Current at 27-degrees-N derived from cross-stream voltages and profiling data—Theory and observations. *Phil. Trans. R. Soc. Lond. A* **338,** 169–236 (1992).
5. Kim, S. T. & O'Neil, J. R. Equilibrium and nonequilibrium oxygen isotope effects in synthetic carbonates. *Geochim. Cosmochim. Acta* **61,** 3461–3475 (1997).
6. Craig, H. & Gordon, L. I. in *Pro. 3rd Spoleto Conf., Spoleto, Italy* (ed. Tongiori, E.) 9–130 (Sischi and Figli, Pisa, 1965).
7. Slowey, N. C. & Curry, W. B. Glacial-interglacial differences in circulation and carbon cycling within the upper western North-Atlantic. *Paleoceanography* **10,** 715–732 (1995).
8. Haddad, G. A. & Droxler, A. W. Metastable $CaCO_3$ dissolution at intermediate water depths of the Caribbean and western North Atlantic: Implications for intermediate water circulation during the past 200,000 years. *Paleoceanography* **11,** 701–716 (1996).
9. Marchitto, T. M., Curry, W. B. & Oppo, D. W. Millennial-scale changes in North Atlantic circulation since the last glaciation. *Nature* **393,** 557–561 (1998).
10. Kutzbach, J. *et al.* Climate and biome simulations for the past 21,000 years. *Quat. Sci. Rev.* **17,** 473–506 (1998).
11. Seidov, D., Sarnthein, M., Strattegger, K., Prien, R. & Weinelt, M. North Atlantic ocean circulation during the last glacial maximum and subsequent meltwater event: A numerical model. *J. Geophys. Res.* **101,** 16305–16332 (1996).
12. Boyle, E. A. & Keigwin, L. D. North Atlantic thermohaline circulation during the last 20,000 years linked to high latitude surface temperature. *Nature* **330,** 35–40 (1987).
13. Duplessy, J.-C. *et al.* Deepwater source variation during the last climatic cycle and their impact on global deepwater circulation. *Paleoceanography* **3,** 343–360 (1988).
14. Sarnthein, M. *et al.* Changes in east Atlantic deep-water circulation over the last 30,000 years—8 time slice reconstructions. *Paleoceanography* **9,** 209–267 (1994).
15. Oppo, D. W. & Lehman, S. J. Mid-depth circulation of the subpolar North-Atlantic during the Last Glacial Maximum. *Science* **259,** 1148–1152 (1993).
16. Fichefet, T., Hovine, S. & Duplessy, J.-C. A model study of the Atlantic thermohaline circulation during the last glacial maximum. *Nature* **372,** 252–255 (1994).
17. Ganopolski, A., Rahmstorf, S., Petoukhov, V. & Claussen, M. Stimulation of modern and glacial climates with a coupled global model of intermediate complexity. *Nature* **391,** 351–356 (1998).
18. Sigman, D. M. & Lehman, S. J. in *American Geophysical Union Fall Meeting* (AGU, San Francisco, California, 1995).
19. Yu, E. F., Francois, R. & Bacon, M. P. Similar rates of modern and last-glacial ocean thermohaline circulation inferred from radiochemical data. *Nature* **379,** 689–694 (1996).
20. Lynch-Stieglitz, J., vanGeen, A. & Fairbanks, R. G. Interocean exchange of Glacial North Atlantic intermediate water: Evidence from Subantarctic Cd/Ca and carbon isotope measurements. *Paleoceanography* **11,** 191–201 (1996).
21. Winguth, A. M. E., Archer, D., Duplessy, J.-C., Maier-Reimer, E. & Mikolajewicz, U. Sensitivity of paleonutrient tracer distributions and deep-sea circulation to glacial boundary conditions. *Paleoceanography* **14,** 304–323 (1999).
22. McIntyre, A. *et al.* in *Investigation of Late Quaternary Paleo-Oceanography and Paleoclimatology* (eds Cline, R. M. & Hays, J. D.) 43–76 (The Geological Society of America, Boulder, 1976).
23. Labeyrie, L. D. *et al.* Changes in the vertical structure of the North-Atlantic Ocean between glacial and modern times. *Quat. Sci. Rev.* **11,** 401–413 (1992).
24. Curry, W. B. in *The South Atlantic: Present and Past Circulation* (eds Wefer, G., Berger, W. H., Siedler, G. & Webb, D.) (Springer, New York, 1996).
25. Slowey, N. C. & Curry, W. B. Enhanced ventilation of the North Atlantic subtropical gyre thermocline during the last glaciation. *Nature* **358,** 665–668 (1992).
26. Fairbanks, R. G. A 17,000-year glacio-eustatic sea-level record—Influence of glacial melting rates on the Younger Dryas Event and deep-ocean circulation. *Nature* **342,** 637–642 (1989).
27. Schrag, D. P., Hampt, G. & Murray, D. W. Pore fluid constraints on the temperature and oxygen isotopic composition of the glacial ocean. *Science* **272,** 1930–1932 (1996).

28. Joussaume, S. & Jouzel, J. Paleoclimatic tracers—An investigation using an atmospheric general-circulation model under ice-age conditions. 2. Water isotopes. *J. Geophys. Res. Atmos.* **98,** 2807–2830 (1993).
29. Levitus, S. & Boyer, T. P. *World Ocean Atlas 1994* (National Oceanic and Atmospheric Administration, Washington DC, 1994).
30. Leaman, K. D., Johns, E. & Rossby, T. The average distribution of volume transport and potential vorticity with temperature at 3 sections across the Gulf-Stream. *J. Phys. Oceanogr.* **19,** 36–51 (1989).
31. Slowey, N. C. *et al.* Glacial to Holocene sedimentation on the western slope of Great Bahama Bank. *Geo-Mar. Lett.* (submitted).

Acknowledgements

This work was supported by grants from the US National Science Foundation and a grant/cooperative agreement from the National Oceanic and Atmospheric Administration. The views expressed herein are those of the authors and do not necessarily reflect the views of NOAA or any of its subagencies. Support for the curating facilities of the Lamont-Doherty Earth Observatory Deep-Sea Sample Repository is provided by the National Science Foundation and the Office of Naval Research. We are grateful to J. Mayer, A. LeGrande, D. Ostermann and M. Yeager for technical assistance.

Correspondence and requests for materials should be addressed to J.L.-S. (e-mail: jean@ldeo.columbia.edu).

A criterion for the fragmentation of bubbly magma based on brittle failure theory

Youxue Zhang

Department of Geological Sciences, The University of Michigan, Ann Arbor, Michigan 48109-1063, USA

The fragmentation of bubbly magma is a defining point in a volcanic eruption—before fragmentation the magma flows relatively slowly, during fragmentation the bubbles break up to release compressed gas and, afterwards, the eruption becomes a violent gas flow carrying suspended magma particles. Seemingly benign lava flows or domes can suddenly fragment into deadly pyroclastic flows[1–3]. Several criteria have been proposed to define the point of magma fragmentation or foam stability[4–7]. The criterion of Papale[7] is based on melt relaxation theory and equates magma strain rate with the rate of increase of flow velocity with distance. It ignores, however, the role of bubble pressure in causing fragmentation. Two empirical approaches[4,5] consider the role of high bubble pressure in causing fragmentation but do not address the underlying physics of magma fragmentation. Here I develop a fragmentation criterion for bubbly magma based on brittle failure theory and apply it to the fragmentation of lava domes and flows. On the basis of this theory, a bubbly magma will fragment when the tensile stress at the inner walls of bubbles exceeds the tensile strength of the magma. The fragmentation conditions depend strongly on initial water content, with calculated vesicularity and final water levels coinciding reasonably well with those in observed pumices. This suggests that the proposed criterion captures the essence of the fragmentation process in bubbly magma.

Table 1 Calculated conditions for fragmentation

Given conditions				Fragmentation conditions	
T (°C)	S (bar)	P_{out} (bar)	$H_2O_{t,i}$ (wt%)	Vesicularity (%)	$H_2O_{t,av}$ (wt%)
700	60	1	1.0	57	0.66
700	60	3	1.0	63	0.63
700	50	1	1.0	47	0.74
700	50	1	0.7	77	0.35

$H_2O_{t,av}$ is the average H_2O_t in the melt shell at the time of fragmentation.

Fragmentation can be viewed as the result of brittle failure of many bubbles at roughly the same time. Hartog[8] summarized classic theories of material strength and concluded that (1) the maximum-strain theory has been discredited by experiments; (2) the maximum-stress theory applies well to the failure of brittle materials; and (3) the maximum-shear theory applies well to the beginning of yield in ductile materials. The maximum-stress theory states that brittle failure occurs when the maximum tensile stress (σ_{max}) exceeds the tensile strength of the material (S):

$$\sigma_{max} > S \quad (1)$$

In modern treatment of fracture mechanics, brittle failure occurs when the stress intensity factor exceeds the fracture toughness[9]. The stress intensity factor can be calculated, given the size and shape of any microcrack or visible crack. However, because the distribution, size, and shape of the initial microcracks and weaknesses are not known *a priori* in a magma, it is difficult to apply the modern approach. Nevertheless, the application of modern fracture mechanics arguments to a material containing numerous random small cracks leads to the modified Mohr theory of failure, which is equivalent to the maximum-stress theory if the sum of the greatest and least principal stresses is positive (J. R. Barber, personal communication). Because the maximum-stress theory is relatively easy to apply, it will be used in this work.

A bubbly magma system is complicated by the non-uniform distribution of bubbles of variable sizes. A first-order approximation is to assume that all bubbles are spherical, of the same size, and spaced regularly (Fig. 1a). Because the stress distribution and bubble growth rate in this case is still too complicated, it is further approximated by assuming that each spherical bubble is surrounded by a spherical shell (Fig. 1b), for which an analytical solution of stress distribution can be obtained and a numerical solution of bubble growth is available. Where the pressure at the outside surface of the shell is P_{out} and the pressure in the bubble is P_{in}, the stress at the bubble wall (inner wall of the shell) can be expressed as[10]:

$$\sigma^{rr} = -P_{in} \quad (2)$$

$$\sigma^{tt} = (P_{in} - P_{out})\frac{1+2x}{2(1-x)} - P_{out} \quad (3)$$

Here σ^{rr} is the radial stress (and one of the principal stresses), σ^{tt} is the tangential stress (and two of the principal stresses), and x is vesicularity. Tensile stress is positive and compressive stress is negative. $(P_{in} - P_{out})$ is referred to as ΔP hereafter and can be identified as the dynamic pressure, P_{dyn} (refs 11, 12). That ΔP is non-zero means that stress in the magma is not dissipated by viscous flow. That is, the fragmentation criterion for bubbly magma using the maximum-stress theory also automatically incorporates consideration of the liquid–glass transition.

When $P_{in} > P_{out} > 0$, then σ^{rr} is compressive and σ^{tt} can be tensile. The fracture criterion under compressive stresses is more complicated and is not considered here. When $\sigma^{tt} + \sigma^{rr}$ is positive, the maximum-stress theory applies. The maximum tensile stress is the tangential stress at the bubble wall (σ^{tt} above). When the maximum tensile stress (σ^{tt}) exceeds the tensile strength of the melt, the shells surrounding bubbles fail. That is, brittle failure occurs when the following holds:

$$\frac{1+2x}{2(1-x)}\Delta P - P_{out} > S \quad (4)$$

Increasing P_{in} or increasing x (that is, decreasing the shell thickness) increases the tensile stress, and hence increases the likelihood of brittle failure. Because the crack volume is small and because P_{in} is exerted by the gas, the development of cracks does not significantly reduce ΔP and hence does not relieve the stress. Therefore, the cracks will grow until the bubble wall is broken (and the stress is thus relieved). This is in contrast to cracking